Available online at www.sciencedirect.com
ScienceDirect
Physics Letters B 647 (2007) 111–117
PHYSICS LETTERS B
www.elsevier.com/locate/physletb

Relativistic RPA plus phonon-coupling analysis of pygmy dipole resonances

E. Litvinova [a,b], P. Ring [a], D. Vretenar [a,c,*]

[a] *Physik-Department der Technischen Universität München, Germany*
[b] *Institute of Physics and Power Engineering, 249020 Obninsk, Russia*
[c] *Physics Department, Faculty of Science, University of Zagreb, Croatia*

Received 25 July 2006; received in revised form 16 January 2007; accepted 18 January 2007

Available online 16 February 2007

Editor: J.-P. Blaizot

Abstract

The relativistic random-phase approximation (RRPA) plus phonon-coupling (PC) model is applied in the analysis of E1 strength distributions in ^{208}Pb and ^{132}Sn, for which data on pygmy dipole resonances (PDR) have recently been reported. The covariant response theory is fully consistent: the effective nuclear interaction NL3 is used both to calculate the spectrum of single-nucleon Dirac states, and as the residual interaction which determines the collective phonon states in the relativistic RPA. It is shown that the picture of the PDR as a resonant oscillation of the neutron skin against the isospin saturated proton–neutron core, and with the corresponding RRPA state characterized by a coherent superposition of many neutron particle–hole configurations, remains essentially unchanged when particle–vibration coupling is included. The effect of two-phonon admixtures is a weak fragmentation and a small shift of PDR states to lower excitation energy. Even though the PDR calculated in the extended model space of $ph \otimes$ phonon configurations contains sizeable two-phonon admixtures, it basically retains a one-phonon character and its dynamics is not modified by the coupling to low-lying surface vibrations.

PACS: 21.30.Fe; 21.60.Jz; 24.30.Cz; 24.30.Gd

The multipole response of nuclei far from the β-stability line and the possible occurrence of exotic modes of excitation has been the subject of a number of recent theoretical and experimental studies. For neutron-rich nuclei in particular, the pygmy dipole resonance (PDR), i.e. the resonant oscillation of the weakly-bound neutron skin against the isospin saturated proton–neutron core has been investigated. The onset of low-lying E1 strength has been observed not only in exotic nuclei with a large neutron excess, e.g. for neutron-rich oxygen isotopes [1], but also in stable nuclei with moderate proton–neutron asymmetry, like ^{44,48}Ca and ^{208}Pb [2–4]. Very recently the dipole strength distribution above the one-neutron separation energy was also measured in the unstable ^{130}Sn and the doubly-magic ^{132}Sn [5]. In addition to the giant dipole resonance (GDR), evidence was reported for a PDR structure at excitation energy around 10 MeV both in ^{130}Sn and ^{132}Sn, exhausting a few percent of the E1 energy-weighted sum rule.

The interpretation of the dynamics of observed low-lying E1 strength in nuclei with a pronounced neutron excess is very much under discussion. Virtually all theoretical analyses, including shell-model studies and a number of models based on the random-phase approximation (RPA), have shown that in light nuclei, e.g. in neutron-rich oxygen isotopes, the low-lying dipole strength is not collective and originates from non-resonant single-neutron excitations. The situation is different in medium-heavy and heavy nuclei, where the occurrence of collective PDR states has been predicted by several RPA-based calculations, whereas other studies, including also RPA-based models, did not find collective pygmy states in the energy region below the GDR, but only dipole states characterized by single-neutron particle–hole configurations. In particular, studies based on the relativistic RPA [6–9] have shown that in neutron-rich nuclei the electric dipole response is characterized by the fragmentation of the strength distribution and its spreading into the low-energy region. In contrast to light nu-

* Corresponding author at: Physics Department, Faculty of Science, University of Zagreb, Croatia.
E-mail address: dario.vretenar@ph.tum.de (D. Vretenar).

0370-2693/$ – see front matter
doi:10.1016/j.physletb.2007.01.056

clei where the onset of dipole strength in the low-energy region is due to non-resonant single-particle excitations of the loosely bound neutrons, in relativistic RPA calculations of heavier nuclei low-lying dipole states appear which display a more distributed structure of the RPA amplitudes. For these nuclei a single collective dipole state is identified in the low-energy region, and the characteristic dynamics of the pygmy resonance becomes apparent from the analysis of the corresponding transition densities and velocity distributions. The relativistic RPA analysis of Ref. [6] predicted the PDR in ^{208}Pb at an excitation energy close to the neutron emission threshold, and subsequently such a resonant structure was identified in a high-resolution (γ, γ') study [2], with a centroid energy precisely at the neutron threshold ($E_{th} = 7.37$ MeV). In Refs. [7–9] the relativistic RPA and quasiparticle (Q)RPA were employed in the analysis of the E1 response in Sn isotopes, and the occurrence of the PDR was predicted in neutron-rich Sn nuclei. This prediction was confirmed in the recent Coulomb dissociation experiment reported in Ref. [5], in which the PDR structure was observed in ^{130}Sn and ^{132}Sn.

The relativistic RPA and QRPA analyses of the dynamics of low-lying E1 strength distributions described above were performed on the mean-field level, i.e. without taking into account the spreading effects which arise from the coupling of single-nucleon states to the collective low-lying excitations (phonons). The principal effect of the particle–vibration coupling is an increase of the nucleon effective mass at the Fermi surface, and this is reflected in an increase of the density of single-nucleon states close to the Fermi energy. It has been argued that the inclusion of particle–vibration coupling in (Q)RPA calculations, i.e. extending the (Q)RPA model space to include selected two-quasiparticle ⊗ phonon states, would not only improve the agreement between the calculated and empirical widths of the GDR structures, but it could also have a pronounced effect on the low-lying E1 strength. For instance, the coupling to low-lying phonons could fragment the PDR structure over a wide region of excitation energies. As a result of this fragmentation only an enhancement of the E1 strength would be observed in the low-energy region, rather than a prominent PDR peak. The importance of particle–vibration coupling effects for the multipole response of neutron-rich nuclei has particularly been emphasized in studies that have used the QRPA plus phonon coupling model based on the Hartree–Fock (Q)RPA with Skyrme effective forces [10,11]. For the neutron-rich oxygen isotopes it was shown that the experimentally observed dipole strength below 15 MeV [1] could not be reproduced with a simple QRPA calculation, but only with the inclusion of the coupling with phonons [10]. In Ref. [11] the QRPA plus phonon coupling model was applied in the analysis of dipole excitations in ^{208}Pb, ^{120}Sn and ^{132}Sn. In contrast to the results obtained in the relativistic (Q)RPA framework, the QRPA plus phonon coupling model predicts low-lying E1 strength of non-collective nature in all three nuclei. In particular, from the analysis of the structure of RPA amplitudes, it was concluded that none of the four peaks lying below 10 MeV in ^{132}Sn contains contributions of more than two or three different neutron particle–hole (ph) configurations. Predominantly these peaks correspond to just a single-neutron transition, and each of them exhausts less than 0.5% of the energy-weighted sum rule. Low-lying E1 excitations in neutron-rich Sn isotopes have also been studied in the quasiparticle phonon model (QPM) [12], in a model space that included up to three-phonon configurations built from a basis of QRPA states, and with separable multipole–multipole residual interactions. The single-nucleon spectra were calculated for a Woods–Saxon potential with adjustable parameters. Empirical couplings were used for the QPM residual interactions. In the QPM spectra for $^{120-132}$Sn the low-energy dipole strength was found concentrated in a narrow energy interval such that the PDR could be identified. A dependence of the PDR strength and centroid energies on the neutron-skin thickness was analyzed. It was shown that, despite significant multi-phonon contributions to the mean-energy and transition strength, the PDR states basically retain their one-phonon character.

In this work we report the first application of the relativistic RPA plus phonon-coupling model in the calculation of the E1 strength distribution in ^{208}Pb and ^{132}Sn. The relativistic mean-field framework has recently been extended to include the coupling of single-nucleon states to low-lying vibrational states (phonons), and its effect on the single-nucleon spectra has been analyzed [13]. In the present study we employ a fully consistent covariant response theory, which uses the particle–vibration coupling model in the time-blocking approximation (TBA) [14–17] to describe the spreading widths of multipole giant resonances in even–even spherical nuclei. In the TBA a special time-projection technique is used to block the propagation of ph configurations through states which have a more complex structure than $ph \otimes$ phonon. The nuclear response can then be explicitly calculated on the $ph \otimes$ phonon level by summation of infinite series of Feynman's diagrams.

The linear response function is the solution of the Bethe–Salpeter equation (BSE) in the particle–hole (ph) channel

$$R(14,23) = \tilde{G}(1,3)\tilde{G}(4,2) + \frac{1}{i}\sum_{5678} \tilde{G}(1,5)\tilde{G}(6,2)W(58,67)R(74,83), \quad (1)$$

where the notation for the single-particle quantum numbers includes the set of Dirac quantum numbers $\{k_1\}$ and the time variable t_1: $1 = \{k_1, t_1\}$, and the summation implies also integration over the respective time variables. In addition to the usual particle–hole pairs, the configuration space must also include pair-configurations built from positive-energy states occupied in the ground-state solution, and empty negative-energy states in the Dirac sea [18]. Thus the set $\{k_i\}$ includes both positive- and negative-energy states. The dimension of the configuration space is truncated in such a way that the unperturbed particle–hole (antiparticle–hole) energies are smaller than 100 MeV (larger than −1800 MeV) with respect to the positive-energy continuum. The model equations are solved by expanding the nucleon spinors in a spherical harmonic oscillator basis [19]. In the present calculation we have used a basis of 20 oscillator shells.

The amplitude of the ph-interaction W in Eq. (1) reads:

$$W(14,23) = U(14,23) + i\,\Sigma^e(1,3)\tilde{G}^{-1}(4,2) + i\,\tilde{G}^{-1}(1,3)\,\Sigma^e(4,2) - i\,\Sigma^e(1,3)\,\Sigma^e(4,2), \quad (2)$$

where $\tilde{G}$ denotes the mean-field single-particle Green's function

$$\tilde{G}(1,2) = -i\sigma_{k_1}\delta_{k_1k_2}\theta(\sigma_{k_1}\tau)e^{-i\varepsilon_{k_1}\tau}, \quad \tau = t_1 - t_2, \quad (3)$$

and $\sigma_k = \pm 1$ when k denotes an unoccupied (occupied) state. Σ^e is the energy-dependent part of the relativistic mass operator in the Dyson equation for the single-particle propagator [13]. The origin of this energy dependence is the coupling of single-nucleon motion to low-lying collective vibrations, whose energies and amplitudes are calculated with the self-consistent relativistic RPA [18]. U is the amplitude of the effective interaction irreducible in the ph channel. This amplitude is determined as a functional derivative of the total nucleon self-energy Σ with respect to the exact single-particle Green's function:

$$U(14,23) = i\frac{\delta\Sigma(4,3)}{\delta G(2,1)}, \quad (4)$$

and it can be written as a sum of the static mean-field term and a time-dependent term:

$$U(14,23) = V_{k_1k_4,k_2k_3}\delta(t_{31})\delta(t_{21})\delta(t_{34}) + U^e(14,23), \quad (5)$$

where $t_{12} = t_1 - t_2$, and

$$U^e(14,23) = i\frac{\delta\Sigma^e(4,3)}{\delta G(2,1)}. \quad (6)$$

The details of the solution of the Bethe–Salpeter equation (1) in the time-blocking approximation are described in Ref. [20]. From the linear response $R(E)$ the strength function $S(E)$ is calculated for an external field represented by a one-body operator P:

$$S(E) = -\frac{1}{\pi}\lim_{\Delta\to+0}\mathrm{Im}\sum_{k_1k_2k_3k_4} P_{k_2k_1}R_{k_1k_4,k_2k_3}(E+i\Delta)P^*_{k_4k_3}, \quad (7)$$

where the summation is carried out over the whole Dirac space of single-nucleon states, including negative-energy states in the Dirac sea.

The present implementation of the relativistic RPA plus phonon-coupling model is fully consistent: the same covariant energy functional is used to determine (i) the spectrum of positive- and negative-energy single-nucleon states from the self-consistent solution of the corresponding system of Dirac and Klein–Gordon equations, and (ii) to calculate the collective phonon states in the relativistic RPA. These two sets of solutions form the basis for the $ph \otimes$ phonon configurations which determine (iii) the particle–phonon coupling amplitudes. In the present study we have used the density functional based on the standard non-linear effective interaction NL3 [21] in the calculation of the dipole response of ^{208}Pb and ^{132}Sn. The corresponding RPA phonon spaces include collective states with spin and parity: 2^+, 3^-, 4^+, 5^-, and 6^+, with excitation energies below the neutron separation energy B_n, and with a reduced transition probability to the ground state at least 10% of the maximal one for a given spin and parity. For ^{132}Sn this criterion includes all the phonons 2^+, 3^-, 4^+, 5^-, and 6^+ below B_n, whereas in the case of ^{208}Pb a few very weak modes have not been included in the phonon space.

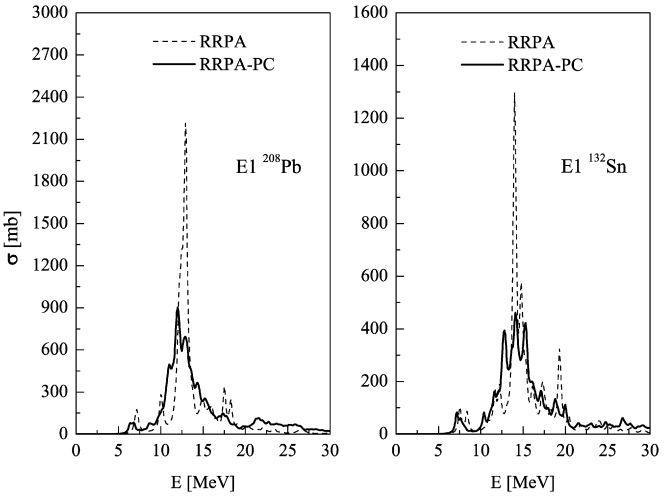

Fig. 1. E1 photoabsorption cross section for ^{208}Pb and ^{132}Sn, calculated with the relativistic RPA (dashed), and with the RRPA extended by the inclusion of particle–phonon coupling (solid).

Table 1
Lorentz fit parameters in the two energy intervals: B_n–25 MeV and 0–30 MeV, for the E1 photoabsorption cross sections in ^{208}Pb and ^{132}Sn, calculated with the RRPA, and with the RRPA extended to include particle–phonon coupling (RRPA-PC), compared to data

		B_n–25 MeV			0–30 MeV		
		$\langle E\rangle$ (MeV)	Γ (MeV)	EWSR (%)	$\langle E\rangle$ (MeV)	Γ (MeV)	EWSR (%)
^{208}Pb	RRPA	13.1	2.4	121	12.9	2.0	128
	RRPA-PC	12.9	4.3	119	13.2	3.0	128
	Exp. [22]	13.4	4.1	117			125(8)
^{132}Sn	RRPA	14.7	3.3	116	14.5	2.6	126
	RRPA-PC	14.4	4.0	112	14.6	3.2	126
	Exp. [5]	16.1(7)	4.7(2.1)	125(32)			

The dipole photoabsorption cross sections

$$\sigma_{E1}(E) = \frac{16\pi^3e^2}{9\hbar c}ES_{E1}(E) \quad (8)$$

for ^{208}Pb and ^{132}Sn, calculated with the smearing parameter $\Delta = 200$ keV are shown in Fig. 1. The corresponding Lorentz fit parameters in the two energy intervals: B_n–25 MeV and 0–30 MeV are included in Table 1, in comparison with data [5,22]. We notice that the inclusion of particle–phonon coupling in the RRPA calculation induces a pronounced fragmentation of the photoabsorption cross sections, and brings the width of the GDR in much better agreement with the data, both for ^{208}Pb and ^{132}Sn.

In this work we are more concerned with the effect of particle–phonon coupling on the E1 strength function in the low-energy region below 10 MeV. The PDR structures predicted by our relativistic RPA calculations for ^{208}Pb [6], and for ^{132}Sn [7,8], are clearly visible in the cross sections of Fig. 1,

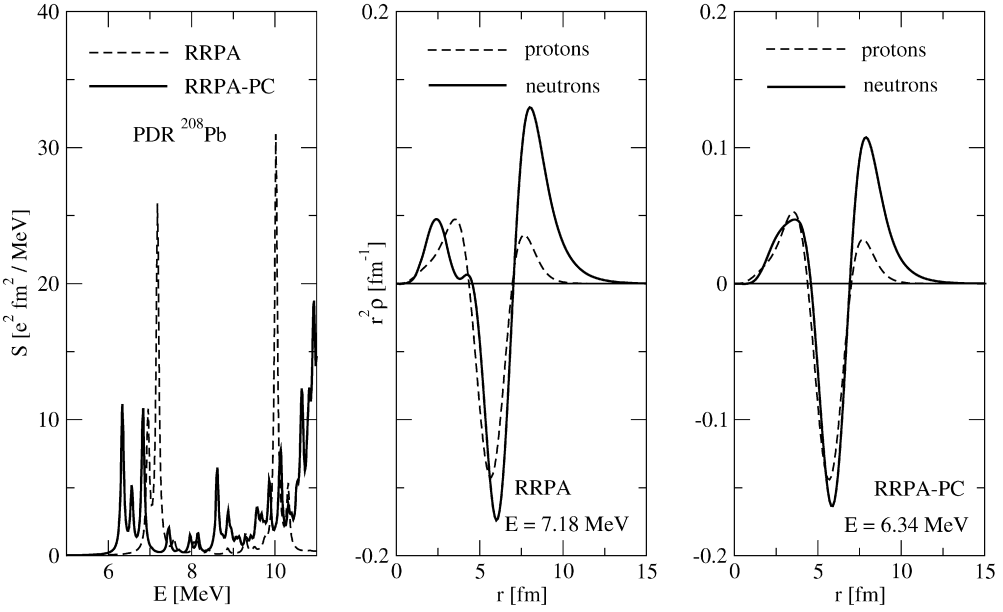

Fig. 2. The low-energy portion of the E1 strength distribution in ^{208}Pb, calculated with the relativistic RPA (dashed), and with the RRPA extended by the inclusion of particle–phonon coupling (solid, RRPA-PC). In the panels on the right the proton and neutron transition densities for the main peaks below 10 MeV, calculated with the RRPA and RRPA-PC, respectively, are plotted as functions of the radial coordinate.

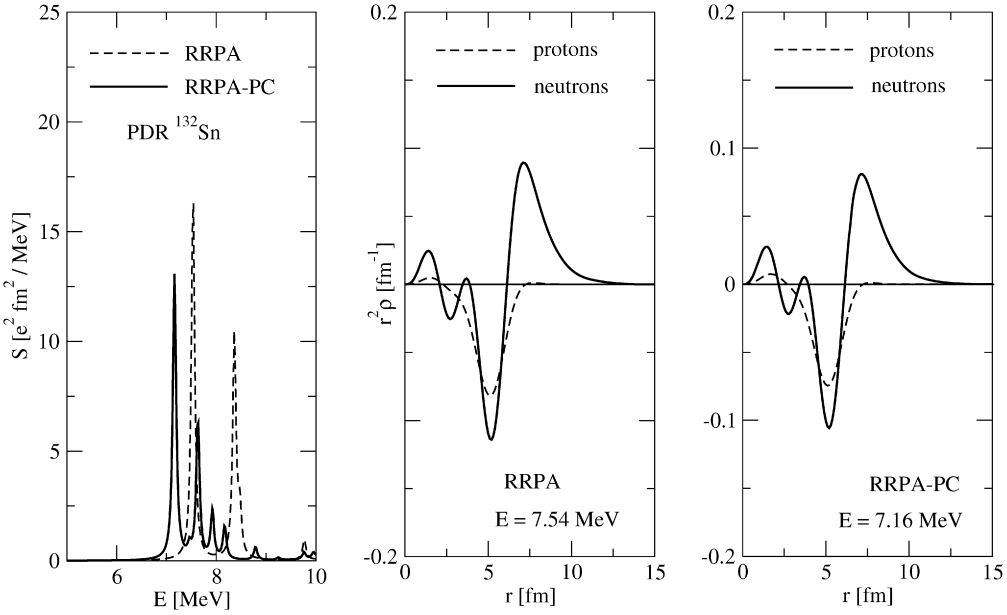

Fig. 3. Same as in Fig. 2, but for ^{132}Sn. The proton and neutron transition densities correspond to the PDR peaks at 7.54 MeV (RRPA) and 7.16 MeV (RRPA-PC).

and we also notice that the inclusion of phonon coupling seems to have a pronounced effect on these structures. The details are shown in Fig. 2 for ^{208}Pb, and in Fig. 3 for ^{132}Sn, where we display the corresponding E1 strength distributions in the low-energy region, calculated with a smaller value of the smearing parameter $\Delta = 40$ keV, together with the proton and neutron transition densities for the strongest peaks below 10 MeV. The PDR peaks calculated with the RRPA display characteristic transition densities that are very different from those of the GDR: the proton and neutron transition densities are in phase in the nuclear interior, there is very little contribution from the protons in the surface region, the isoscalar transition density dominates over the isovector one in the interior, and the large neutron component in the surface region contributes to the formation of a node in the isoscalar transition density. The low-lying pygmy dipole resonance (PDR) does not belong to statistical E1 excitations sitting on the tail of the GDR, but represents a fundamental structure effect: the neutron skin oscillates against the core. This picture remains essentially unchanged by the inclusion of particle–phonon coupling. The principal effect of the coupling with phonons in the low-energy region is the redistribution of the E1 strength and a shift toward lower energies. The main peaks, however, retain their basic dynamics, as it can be seen from the proton and neutron transition densities. In ^{132}Sn, in

Table 2
Distribution of neutron particle–hole configurations for the state at 7.18 MeV (calculated with the RRPA), and for the states at 6.84 MeV and 6.34 MeV (calculated with the RRPA-PC) in ^{208}Pb. See text for the description

RRPA, 7.18 MeV	RRPA-PC, 6.84 MeV	RRPA-PC, 6.34 MeV
23.9% (3p3/2 → 3d5/2)	40.3% (3p3/2 → 3d5/2)	21.5% (2f7/2 → 2g9/2)
22.0% (3p1/2 → 3d3/2)	14.8% (2f7/2 → 2g9/2)	14.5% (1i13/2 → 1j15/2)
10.8% (1i13/2 → 1j15/2)	7.6% (3p1/2 → 3d3/2)	4.2% (3p3/2 → 3d5/2)
6.6% (3p3/2 → 4s1/2)	3.4% (2f5/2 → 3d3/2)	3.1% (3p1/2 → 3d3/2)
4.2% (3p1/2 → 4s1/2)	3.0% (3p3/2 → 4s1/2)	1.2% (3p3/2 → 4s1/2)
2.9% (3p3/2 → 3d3/2)	2.2% (2f5/2 → 3d5/2)	1.2% (1h9/2 → 1i11/2)
2.6% (2f5/2 → 3d3/2)	1.0% (3p3/2 → 3d3/2)	1.0% (1h9/2 → 2g7/2)
2.5% (1h9/2 → 1i11/2)	0.3% (1h9/2 → 1i11/2)	0.8% (3p3/2 → 3d3/2)
2.5% (2f7/2 → 2g9/2)	0.2% (2i13/2 → 1j15/2)	0.7% (2f5/2 → 2g7/2)
0.7% (1h9/2 → 2g7/2)	0.1% (2f5/2 → 4d3/2*)	0.3% (1h9/2 → 2g9/2)
0.7% (2f5/2 → 2g7/2)	0.1% (3p3/2 → 4d5/2*)	0.2% (2f7/2 → 3d5/2)
0.3% (2f5/2 → 3d5/2)	0.1% (2f7/2 → 3d5/2)	0.2% (2f5/2 → 3d3/2)
0.3% (2f7/2 → 3d5/2)		0.1% (2f7/2 → 2g7/2)
0.2% (1h9/2 → 2g9/2)		
80.2%	73.1%	49.0%

Table 3
Same as in Table 2, but for the states at 7.54 MeV (calculated with the RRPA), and at 7.16 MeV (calculated with the RRPA-PC) in ^{132}Sn

RRPA, 7.54 MeV	RRPA-PC, 7.16 MeV
53.6% (3s1/2 → 3p3/2)	49.5% (3s1/2 → 3p3/2)
16.5% (3s1/2 → 3p1/2)	21.5% (3s1/2 → 3p1/2)
9.7% (2d3/2 → 3p1/2)	6.4% (2d3/2 → 3p1/2)
7.3% (2d3/2 → 3p3/2)	4.1% (1h11/2 → 1i13/2)
4.7% (1h11/2 → 1i13/2)	3.9% (2d3/2 → 3p3/2)
0.9% (1g7/2 → 1h9/2)	0.7% (1g7/2 → 1h9/2)
0.3% (2d5/2 → 3p3/2)	0.1% (1g7/2 → 2f5/2)
0.2% (1g7/2 → 2f5/2)	0.1% (2d5/2 → 3p3/2)
0.1% (1g7/2 → 2f7/2)	0.1% (2d3/2 → 4p1/2*)
0.1% (2d3/2 → 4p1/2*)	0.1% (1g7/2 → 2f7/2)
	0.1% (3s1/2 → 4p1/2*)
	0.1% (3s1/2 → 4p3/2*)
93.4%	86.7%

particular, the coupling to phonons has the effect of concentrating most of the low-lying strength in the PDR peak at 7.16 MeV.

The effect of particle–vibration coupling on the PDR states is also illustrated in Table 2 for ^{208}Pb, and in Table 3 for ^{132}Sn, where we display the distributions of the neutron particle–hole configurations for the most prominent PDR peaks calculated with the RRPA, and with the RRPA-PC model. We only include configurations which contribute more than 0.1% to the total RRPA amplitude. For the states calculated with the RRPA the percentage assigned to a particular ph configuration refers to the usual normalization of the RRPA amplitudes for an excited state $|\nu\rangle$:

$$\sum_{ph}\left(\left|\rho^{\nu}_{ph}\right|^2-\left|\rho^{\nu}_{hp}\right|^2\right)=1. \tag{9}$$

We first notice that both in ^{208}Pb and ^{132}Sn, many neutron ph configurations contribute to the RRPA amplitudes of the PDR peaks. In ^{208}Pb we find 14 configurations with more than 0.1% of the total amplitude, with the largest being (3p3/2 → 3d5/2) with 23.9%. These 14 configurations together contribute 80.2% to the total amplitude, and the remaining ≈ 20% is the contribution of proton configurations, and weak neutron ph-states with amplitudes < 0.1%. Note that for GDR states the ratio of neutron to proton contribution to the RPA amplitude is typically N/Z, i.e. ≈ 1.5 for ^{208}Pb, whereas this ratio is more than 4 for the PDR state. An extreme case is the PDR at 7.54 MeV in ^{132}Sn (Table 3), for which the 10 largest neutron ph amplitudes contribute more than 93% to the total RRPA amplitude. The difference between the proton contributions to the PDR in ^{208}Pb and ^{132}Sn is also seen in the corresponding transition densities shown in Figs. 2 and 3.

In order to derive the normalization condition for the RRPA plus phonon-coupling model, let us rewrite the BS Eq. (1) by using the time-projection in the TBA [14–17], and performing the Fourier transformation to the energy domain:

$$\begin{aligned}&R_{k_1k_4,k_2k_3}(\omega)\\&\quad=\tilde{R}_{k_1k_4,k_2k_3}(\omega)\\&\qquad-\sum_{k_5k_6k_7k_8}\tilde{R}_{k_1k_6,k_2k_5}(\omega)\Phi_{k_5k_8,k_6k_7}(\omega)R_{k_7k_4,k_8k_3}(\omega),\end{aligned} \tag{10}$$

where $\tilde{R}$ is the mean-field propagator:

$$\tilde{R}_{k_1k_4,k_2k_3}(\omega)=-\frac{\sigma_{k_1}\delta_{\sigma_{k_1},-\sigma_{k_2}}\delta_{k_1k_3}\delta_{k_2k_4}}{\omega-\varepsilon_{12}}, \tag{11}$$

$\varepsilon_{12}=\varepsilon_{k_1}-\varepsilon_{k_2}$. Φ is the generalized amplitude of ph interaction:

$$\Phi_{k_1k_4,k_2k_3}(\omega)=V_{k_1k_4,k_2k_3}+\Phi^{\text{coupl}}_{k_1k_4,k_2k_3}(\omega). \tag{12}$$

Close to an eigenfrequency Ω^{ν} the response function has a simple pole structure:

$$R^{\nu}_{k_1k_4,k_2k_3}(\omega)=-\frac{\rho^{\nu}_{k_1k_2}\rho^{\nu*}_{k_3k_4}}{\omega-\Omega^{\nu}}. \tag{13}$$

One can therefore derive the transition densities for the excited state $|\nu\rangle$:

$$\rho^{\nu}_{k_1k_2}=\lim_{\Delta\to+0}\sqrt{\frac{\Delta}{\pi S(\Omega^{\nu})}}\,\mathrm{Im}\,\delta\rho_{k_1k_2}\left(\Omega^{\nu}+i\Delta\right), \tag{14}$$

where

$$\delta\rho_{k_1k_2}(\omega) = \sum_{k_3k_4} R_{k_1k_4,k_2k_3}(\omega) P^*_{k_4k_3}. \tag{15}$$

It is convenient to rewrite Eq. (10) in the following form:

$$\sum_{k_5k_6}\big(\tilde{R}^{-1}_{k_1k_6,k_2k_5}(\omega) + \Phi_{k_1k_6,k_2k_5}(\omega)\big) R_{k_5k_4,k_6k_3}(\omega) = \delta_{k_1k_3}\delta_{k_2k_4}\delta_{\sigma_{k_1},-\sigma_{k_2}}. \tag{16}$$

By first substituting Eq. (13) into Eq. (16), and then taking a derivative with respect to ω, we obtain the generalized normalization condition:

$$\sum_{k_1k_2k_3k_4} \rho^{\nu *}_{k_1k_2}\left[\sigma_{k_1}\delta_{\sigma_{k_1},-\sigma_{k_2}}\delta_{k_1k_3}\delta_{k_2k_4} - \frac{d\Phi_{k_1k_4,k_2k_3}}{d\omega}\bigg|_{\omega=\Omega^\nu}\right]\rho^\nu_{k_3k_4} = 1, \tag{17}$$

which, in the limiting case of an energy-independent interaction, reduces to the usual RPA normalization:

$$\sum_{k_1k_2}\sigma_{k_1}\delta_{\sigma_{k_1},-\sigma_{k_2}}\big|\rho^\nu_{k_1k_2}\big|^2 = \sum_{ph}\big(\big|\rho^\nu_{ph}\big|^2 - \big|\rho^\nu_{hp}\big|^2\big) = 1. \tag{18}$$

In the particle–vibration coupling model the derivative in Eq. (17) is a non-positively definite matrix, so that the quantity

$$\sum_{ph}\big(\big|\rho^\nu_{ph}\big|^2 - \big|\rho^\nu_{hp}\big|^2\big) \tag{19}$$

is always less or equal to 1, in analogy to the spectroscopic factor of a single-particle state. The difference represents the contribution of $ph \otimes$ phonon configurations.

Because of the coupling to low-lying phonon states, the RRPA pygmy peak at 7.18 MeV in ^{208}Pb becomes fragmented and the E1 strength is shifted to lower energies. In Table 2 we display the structure of the neutron ph configurations for the two most pronounced peaks calculated with the RRPA-PC model at 6.84 MeV and 6.34 MeV. The contributions of each individual neutron ph configuration to the transition amplitude of the state $|\nu\rangle$ are quantified by $|\rho^\nu_{ph}|^2 - |\rho^\nu_{hp}|^2$ (the percentage refers to the generalized normalization of Eq. (17)), with the amplitudes ρ^ν_{ph} and ρ^ν_{hp} calculated from Eq. (14). 12 ph configurations contribute with more than 0.1% to the state at 6.84 MeV, compared to 13 for the state at 6.34 MeV. The corresponding sums of the amplitudes of the pure neutron ph configurations are now reduced with respect to that of the RRPA peak (80.2%), and this reduction indicates the amount of mixing with low-lying phonon states. The admixture of two-phonon states is especially pronounced for the state at 6.34 MeV: only about 50% of the amplitude corresponds to a one-phonon state. Nevertheless, the proton and neutron transition densities display the characteristic PDR structure (see Fig. 2). We note that the strong neutron component (2f7/2 → 2g9/2) (14.8% for the state at 6.84 MeV and 21.5% for the state at 6.34 MeV), which is very weak in the amplitude of the RRPA pygmy peak at 7.18 MeV (2.5%), originates from the strong RRPA peak at 10.02 MeV. The effect of coupling to phonons is much weaker in ^{132}Sn (see Table 3). The sum of the amplitudes of the 12 neutron ph configurations is reduced by less than 7% with respect to the RRPA calculation. The two-phonon admixture is rather weak, and thus the principal effect of coupling with phonon states is the shift in energy of the PDR state from 7.54 MeV to 7.16 MeV.

Table 4
Integral photoabsorption cross sections for the PDR and GDR, and their ratios calculated with the RRPA and RRPA-PC, in comparison with the experimental values. See text for description

		$\sigma_{(\mathrm{PDR})}$ (mb MeV)	$\sigma_{(\mathrm{GDR})}$ (mb MeV)	$\sigma_{(\mathrm{PDR})}/\sigma_{(\mathrm{GDR})}$
^{208}Pb	RRPA	133	3606	0.037
	RRPA-PC	106	3547	0.030
	Exp. [22]		3487	
^{132}Sn	RRPA	115	2162	0.053
	RRPA-PC	91	2087	0.044
	Exp. [5]	75(57)	2330(590)	0.03(2)

In addition to transitions to bound or quasi-bound states, in Tables 2 and 3 we also include transitions (with $\geqslant 0.1\%$ of the total amplitude) to single-neutron states which belong to the discretized continuum (denoted by the asterisk symbol '$*$'). Since their energies depend on the discretization scheme (size of the box or, in the present case, the number of oscillator shells), transitions to these states do not represent physical excitations. However, we notice that the contribution of the transitions to the discretized continuum is very small, and thus our conclusions about the collectivity of pygmy states do not depend on the treatment of the continuum. This is, of course, to be expected for ^{208}Pb and ^{132}Sn, because these nuclei are very far from the neutron drip-line and thus threshold effects do not play any role in the low-energy multipole response.

The calculated cross sections and the predicted contribution of the pygmy resonance to the total dipole strength are compared with available data in Table 4. We note that the integral cross sections $\sigma_{(\mathrm{GDR})}$ calculated in the energy interval B_n–25 MeV are in very good agreement with the experimental values, both for ^{208}Pb and ^{132}Sn. In order to compare the contributions of the PDR to the total strength, we have integrated the calculated cross sections in the region below 8 MeV (9 MeV) for ^{208}Pb (^{132}Sn). The ratios of the resulting $\sigma_{(\mathrm{PDR})}$ to $\sigma_{(\mathrm{GDR})}$ are listed in the last column of Table 4, and compared with the experimental value 0.03(2) for ^{132}Sn [5]. The calculated values of this ratio are: 0.053 for the RRPA, and 0.044 for the RRPA-PC model.

In conclusion, we have applied the relativistic RPA plus phonon-coupling model in the analysis of low-lying E1 strength distributions in ^{208}Pb and ^{132}Sn, for which data on pygmy dipole resonances (PDR) have recently been reported. The theoretical analysis is fully consistent: the effective nuclear interaction NL3 is used both to determine the spectrum of positive- and negative-energy single-nucleon Dirac states, and as the residual interaction which determines the collective phonon states in the relativistic RPA. The phonon space to which the single-nucleon states are allowed to couple includes phonons with spin and parity: 2^+, 3^-, 4^+, 5^-, and 6^+, with excitation energies below the

neutron separation energy, and with a reduced transition probability to the ground state at least 10% of the maximal one for a given spin and parity. The calculated E1 photoabsorption cross sections, the excitation energies, and widths of the giant dipole resonances (GDR) reproduce the available data. In addition the RRPA also predicts the occurrence of PDR states in the region of low excitation energies below 10 MeV, in agreement with recent experimental results. The PDR represents a resonant oscillation of the neutron skin against the isospin saturated proton–neutron core, and the corresponding RRPA state is characterized by a coherent superposition of many neutron particle–hole configurations. In this work we have shown that this picture remains essentially unchanged when particle–vibration coupling is included. The effect of two-phonon admixtures is a small shift of PDR states to lower excitation energy and, in the case of ^{208}Pb, the PDR strength is fragmented over two or three states. Even though the PDR calculated in the extended model space of $ph \otimes$ phonon configurations contains sizeable two-phonon admixtures, it basically retains a one-phonon character and its dynamics is not modified by the coupling to low-lying surface vibrations.

Acknowledgements

Helpful discussions with V. Tselyaev are gratefully acknowledged. This work has been supported in part by the Bundesministerium für Bildung und Forschung under project 06 MT 193, and by the Croatian Ministry of Science and Education under project 1191005-1010. E.L. and D.V. acknowledge the support of the Alexander von Humboldt-Stiftung.

References

[1] A. Leistenschneider, et al., Phys. Rev. Lett. 86 (2001) 5442.
[2] N. Ryezayeva, et al., Phys. Rev. Lett. 89 (2002) 272502.
[3] J. Enders, et al., Nucl. Phys. A 724 (2003) 243.
[4] T. Hartmann, et al., Phys. Rev. Lett. 93 (2004) 192501.
[5] P. Adrich, et al., Phys. Rev. Lett. 95 (2005) 132501.
[6] D. Vretenar, N. Paar, P. Ring, G.A. Lalazissis, Phys. Rev. C 63 (2001) 047301.
[7] D. Vretenar, N. Paar, P. Ring, G.A. Lalazissis, Nucl. Phys. A 692 (2001) 496.
[8] N. Paar, P. Ring, T. Nikšić, D. Vretenar, Phys. Rev. C 67 (2003) 034312.
[9] N. Paar, T. Nikšić, D. Vretenar, P. Ring, Phys. Lett. B 606 (2005) 288.
[10] G. Coló, P.F. Bortignon, Nucl. Phys. A 696 (2001) 427.
[11] D. Sarchi, P.F. Bortignon, G. Coló, Phys. Lett. B 601 (2004) 27.
[12] N. Tsoneva, H. Lenske, Ch. Stoyanov, Phys. Lett. B 586 (2004) 213.
[13] E. Litvinova, P. Ring, Phys. Rev. C 73 (2006) 044328.
[14] V.I. Tselyaev, Yad. Fiz. 50 (1989) 1252, Soviet J. Nucl. Phys. 50 (1989) 780.
[15] S.P. Kamerdzhiev, G.Ya. Tertychny, V.I. Tselyaev, Phys. Part. Nucl. 28 (1997) 134.
[16] V.I. Tselyaev, Phys. Rev. C 75 (2007) 024306.
[17] E.V. Litvinova, V.I. Tselyaev, nucl-th/0512030.
[18] P. Ring, Z.-Y. Ma, N. Van Giai, D. Vretenar, A. Wandelt, L.-G. Cao, Nucl. Phys. A 694 (2001) 249.
[19] Y.K. Gambhir, P. Ring, A. Thimet, Ann. Phys. 198 (1990) 132.
[20] P. Ring, E.V. Litvinova, V.I. Tselyaev, Phys. Rev. C, submitted for publication.
[21] G.A. Lalazissis, J. König, P. Ring, Phys. Rev. C 55 (1997) 540.
[22] A. Veyssiere, H. Beil, R. Bergere, P. Carlos, A. Lepretre, Nucl. Phys. A 159 (1970) 561.